



Fermi National Accelerator Laboratory

FERMILAB-FN-571

Calculation of Radiation Dose around Shielding Penetrations

A. Van Ginneken

*Fermi National Accelerator Laboratory
P.O. Box 500, Batavia, Illinois 60510*

September 1991



Operated by Universities Research Association Inc. under Contract No. DE-AC02-76CHO3000 with the United States Department of Energy

Disclaimer

This report was prepared as an account of work sponsored by an agency of the United States Government. Neither the United States Government nor any agency thereof, nor any of their employees, makes any warranty, express or implied, or assumes any legal liability or responsibility for the accuracy, completeness, or usefulness of any information, apparatus, product, or process disclosed, or represents that its use would not infringe privately owned rights. Reference herein to any specific commercial product, process, or service by trade name, trademark, manufacturer, or otherwise, does not necessarily constitute or imply its endorsement, recommendation, or favoring by the United States Government or any agency thereof. The views and opinions of authors expressed herein do not necessarily state or reflect those of the United States Government or any agency thereof.

Calculation of Radiation Dose around Shielding Penetrations

A. Van Ginneken

Fermi National Accelerator Laboratory*
P. O. Box 500, Batavia, IL 60510

September 1991

Abstract

A two-step algorithm is introduced into the Monte Carlo program CASIM to calculate radiation dose in the vicinity of shielding penetrations. Calculated results are in reasonable agreement with measurements.

1 Introduction

Programs such as the Monte Carlo (MC) code CASIM [1] allow for quite complicated shielding geometries to be analyzed. In principle, unlimited detail can be introduced but practical considerations encourage one to adhere only to the gross features of the problem geometry. Inclusion of detail not only complicates coding but tends to destroy any approximate symmetries a problem may possess—which may otherwise be exploited to save computation time and simplify analysis. And often it is obvious, on statistical grounds, that even an unreasonably long MC run will not adequately explore some given geometrical detail. Such details are then either omitted or averaged over in such a way as to preserve symmetry.

However, for certain problems the ‘detail’ is not so easily disposed of and such is the case for the topic of this note: the presence of a penetration in a shield, e.g., a duct cutting through the shielding berm from a service building

*Fermi National Accelerator Laboratory is operated by Universities Research Association under contract with the US Department of Energy.

to the accelerator enclosure, or a culvert traversing the berm without entering the tunnel. Often the geometry without penetration can be adequately approximated by a cylindrically symmetric one. Inclusion of the penetration not only destroys the symmetry but it is clear *a priori* that even in a long MC run insufficient particles will be generated with the proper coordinates and direction to adequately explore the penetration and its immediate vicinity. Moreover, radiation safety considerations demand that one confront the 'worst case', i.e., estimate the maximum possible dose [2] rate outside the penetration. Given a maximal beam loss mode, this means varying the location where beam is lost relative to the penetration and thus several such (unreasonably long) MC runs would be required to establish the maximum dose. To make analysis of these problems—particularly those of the worst case dose variety—more tractable this note introduces an algorithm for estimating the exit dose of a penetration within reasonable CPU time, though not without some additional approximations.

The present effort differs markedly from the usual treatment of ducts and labyrinths in accelerator shielding (see, e.g., ref [3]). Two assumptions are basic to the latter: (1) the dose is predominantly due to low energy neutrons, which (2) are introduced (solely) at the entrance of the penetration where (somehow) their dose is assumed to be known. With the help of graphs or empirical formulae this entrance dose is then propagated along the penetration. When these assumptions apply, the procedure no doubt provides a useful approximation. But the assumptions—and hence the procedure—are of limited validity around a high energy accelerator, in particular when attempting to predict a worst case dose. In the example of calculating exit dose for a penetration connecting to the accelerator enclosure due to nearby beam loss, particles contributing to the dose will enter the shaft along its entire extent inside the shield—with most entering over a stretch which is typically a few meters in length. In fact, unless the penetration 'points' at the beam loss or close to it, the entrance component may be small or even negligible. There is also a strong anisotropy to the radiation favoring the beam- and radially outward directions. One thus expects a significant dependence of the exit dose on the orientation of the penetration within the shield, which is absent in the usual labyrinth treatment. Note also that the latter appears completely inapplicable to the culvert case.

In the following section the algorithm is briefly described. In sec. 3 results are compared with measurements of dose outside penetrations due to deliberately induced beam loss. Concluding remarks are in sec. 4.

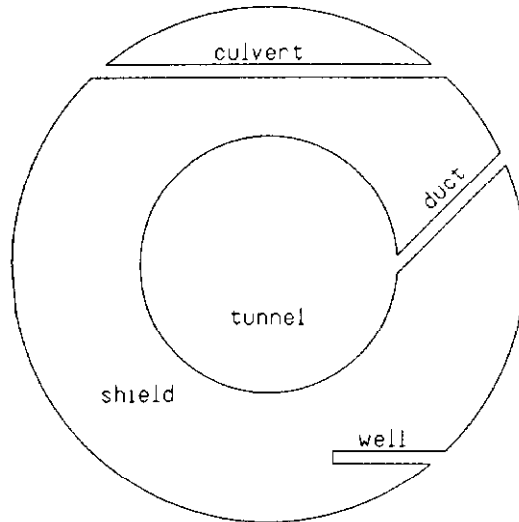


Figure 1: Three prototypes of penetrations encountered in accelerator shielding. Penetrations need not be perpendicular to the beam.

2 Algorithm

Fig. 1 shows three types of straight penetrations, referred to as duct, culvert, and well. Fig. 1 may be interpreted as a projection, i.e., the penetrations need not be at a fixed z (beam direction). Here only straight penetrations of uniform cross section are treated. Extensions to multi-legged ones should be easy to incorporate and are briefly discussed in sec. 4. It is basic to the algorithm that the penetration is *narrow*, i.e., that it does not greatly affect the cascade development and that its radius (or equivalent) is small compared with the tunnel radius. Less basic, but important from statistical considerations, is that one approximates the rest of the geometry with as much (cylindrical) symmetry as possible. The algorithm is described here in terms of the duct case. Culverts and wells require only minor changes which are not elaborated upon.

2.1 CASIM Calculation

The calculation proceeds in two stages. First a CASIM run is performed in a target-in-a-tunnel geometry with a *solid* tunnel wall. The target could be, e.g., a magnet on which beam is lost. Radial dimensions of target and tunnel

are approximated by the actual distance along the beam-to-penetration direction at closest approach or averaged thereabouts over some finite angular range. CASIM then calculates star density as a function of location within the tunnel wall. In addition, the *restricted* star density is accumulated during the MC, where restricted refers to the *direction* of the particle creating the star *with respect its radius vector*. It is required to lie within some small solid angle of the direction made by the penetration with respect to the radius vector at the same radial distance. The restricted star density is thus expressed as a number of stars per unit volume and per unit solid angle. Note that the restriction-direction depends on r , unless the penetration lies along a radius vector. Note also that when full cylindrical symmetry applies the restricted star density calculation makes use of the entire (2π) azimuthal range. Where this is not possible a compromise is made between adherence to the actual geometry and maximizing the azimuthal range for statistical gain.

2.2 Penetration

In the second stage, following the MC, the penetration is introduced explicitly. The basic geometry assumed now is that of a *cylindrical penetration in a slab* representing the shield. Using simple geometric arguments along with the star densities (plain and restricted) from the first stage, the dose at the exit of the penetration is estimated by summing: (1) the dose due to particles above 0.3 GeV/c, derived from the restricted star density, (2) a component—for ducts only—which enters directly from the tunnel, (3) a low energy neutron component which assumes that the (unrestricted) stars emit some low energy neutrons isotropically, and (4) for relatively thin shields the dose at the exit point in the absence of a penetration. Computation of this second stage is very fast and readily repeated at each z -location of the CASIM binning array. If the problem has translation symmetry along the beam direction, a single MC run can thus predict exit dose as a function of distance from beam loss and its maximum represents the worst case dose.

To start, consider, as in fig.2, a duct which is only *partially* evacuated: from the top down to some height, T , above the tunnel ceiling, and consider a slice ΔT of shielding material at the boundary. A particle producing a restricted star within the slice would have continued unimpeded if ΔT were part of the penetration instead of the shield. The total contribution to the

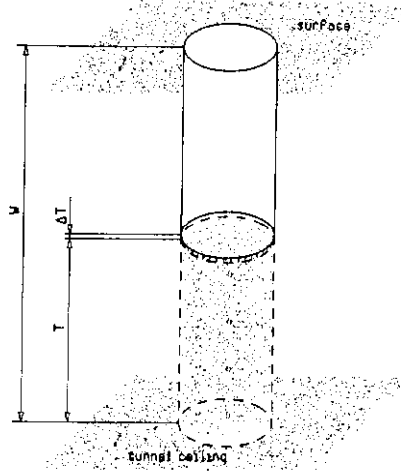


Figure 2: Dose increment from removing top slice ΔT of partially evacuated duct.

dose on top of the duct from ΔT is easily evaluated:

$$D(T) = \frac{\pi r_p^2 \Delta T \rho_*^\phi(T) g(T) c_\phi}{(W - T)^2} \quad (1)$$

where r_p is the radius of the penetration, ρ_*^ϕ is the restricted star density, $g(T)$ is a geometric factor which corrects for the presence of the penetration *below* ΔT , c_ϕ converts flux to dose [4], and W is the total shield thickness. To get the total dose eq. (1) is integrated over T from 0 to W (after the usual $\Delta T \rightarrow dT$).

Using a simple geometric model $g(T)$ assigns to the particles from ΔT , assumed to reach the top within the penetration as per eq. 1, a probability which reflects their place of origin, i.e., the star of the previous generation where they are produced. If all trajectories are straight and ignoring—for the moment—entrance from the tunnel, these particles must have originated somewhere in the truncated conical region beneath ΔT , as indicated in fig. 3. The location of this earlier interaction determines the contribution of the (restricted) star to the dose, viz., it must be (1) completely excluded if inside the penetration and (2) reduced by a ‘shadow factor’ elsewhere. Note that, for clarity, figs. 2 and 3 are not drawn in the strict spirit of the narrow penetration assumption.

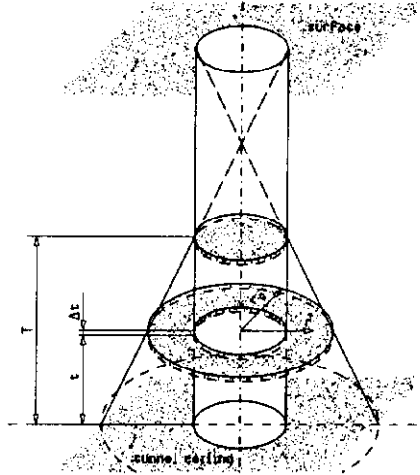


Figure 3: Dose at exit of fully evacuated duct from slice ΔT due to particles originating between t and $t + \Delta t$.

2.3 Shadow Factor

For a particle originating at depth t and lateral position \vec{r} , the shadow factor, S_\wedge , can be defined as the fraction of the penetration lying within the shadow cast by ΔT in the exit plane by a source at t and \vec{r} (see fig. 3). For the purpose of deriving the shadow factor, it is convenient to set r_p , the radius of the penetration, equal to unity and to locate the source point, (t, \vec{r}) , on the z -axis. According to the narrow-penetration-assumption, $r \ll t$, for typical distances around the penetration and the shadow of ΔT in the exit plane which is centered at x_c —the projection of the center of ΔT —will be close to circular in shape, with a radius $\alpha = (W - t)/(T - t)$ times that of the penetration, which is independent of \vec{r} . The overlap of the two circles in the exit plane is then the sum of two contiguous circular segments (see fig. 4) with an area readily obtained by integration:

$$A = \cos^{-1} x_b + \alpha^2 \cos^{-1} \frac{x_c - x_b}{\alpha} - x_c \sqrt{1 - x_b^2} \quad (2)$$

where x_b is measured from the center of the penetration to the common boundary of the two segments. In terms of this area, A , the *average* shadow factor for given t , is then

$$\bar{S}_\wedge(t) = \frac{\int_1^{r_0} A 2\pi r dr}{\pi^2 (r_0^2 - 1)} \quad (3)$$

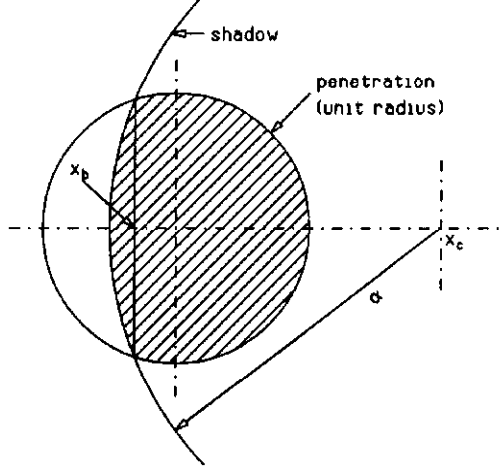


Figure 4: Shadow factor for particles emitted off center.

where $\tau_0 = (\alpha + 1)/(\alpha - 1)$, beyond which contributions from depth, t , vanish. Eq. 3 integrates out to

$$\bar{S}_\wedge(t) = \frac{1}{2} - \frac{1}{4\alpha}. \quad (4)$$

2.4 Shield Dose

The exit dose due to particles produced in the shield which take significant advantage of the penetration (referred to here as the 'shield dose') can now be evaluated from the above ingredients. Based on the narrow penetration approximation, it is assumed that ρ_\star^\varnothing is constant over the angular range of the particles arriving at ΔT from below and varies sufficiently slowly with z to (conveniently) use only the *local* ρ_\star^\varnothing . The probability of origin of the restricted stars in ΔT at T can then be estimated using Bayes' Theorem: [5]

$$P_{\Delta T}(T, t, r) = \frac{\rho_\star^\varnothing(t) \exp(-(T-t)/\lambda) 2\pi r}{\int \int \rho_\star^\varnothing(t) \exp(-(T-t)/\lambda) 2\pi r dr dt}. \quad (5)$$

By applying to eq. 5 the exclusion rule (for $r < 1$) and the shadow factor (for $r \geq 1$) and then integrating over all r and t , $g(T)$ is obtained. The r integration is trivial and there remains:

$$g(T) = \frac{\int \rho_\star^\varnothing(t) \exp(-(T-t)/\lambda) \bar{S}_\wedge(t) \pi (\tau_0^2 - 1) dt}{\int \rho_\star^\varnothing(t) \exp(-(T-t)/\lambda) \pi r_0^2 dt} \quad (6)$$

with the integrations performed numerically. As in a typical CASIM run, star densities (restricted and otherwise) are generated in volume bins over an equispaced (z, r) grid and the numerical integration, eq. 6, is conveniently done in steps corresponding to this grid assuming a constant $\rho_\star^\mathcal{O}(t)$ within such a step. Note that $\Delta t \neq \Delta r$, except for a radial penetration, and Δt involves the z -coordinate when the penetration is not perpendicular to the beam. The exit ‘shield dose’ is obtained by integrating eq. 1 over all T , again numerically and with steps corresponding to the CASIM bin boundaries. [6] For wells a contribution from the bottom of the penetration must be included.

2.5 Tunnel Dose

For ducts, the contribution to the exit dose from particles entering directly from the tunnel and traversing the entire length, W , of the penetration is readily evaluated from the restricted star density in the radial bins adjacent to the tunnel:

$$D(z) = \rho_\star^\mathcal{O}(r_1, z) \pi r_p^2 c_\star / W^2. \quad (7)$$

where r_1 refers to the lowermost r -bin and c_\star converts stars to dose. When Δr of the bin becomes comparable to λ , $\rho_\star^\mathcal{O}(r_1, z)$ may contain stars from particles produced in the shield. In that case it is a simple matter to keep track separately of the true tunnel entrance particles.

The ‘tunnel dose’ is very sensitive to the beam loss- and penetration geometry, especially with respect to the area ‘viewed’ directly by the duct, which must therefore be modeled with some care. Obviously, a large tunnel dose is expected outside of a penetration which points directly at the beamline. Where this is not the case, the distance from the beam loss to the wall opposite the penetration becomes a critical parameter. It may be advantageous, see sec. 3, to calculate this component in a separate MC run with a (cylindrical) geometry which better reflects the cascade trajectories contributing to the tunnel dose.

When the tunnel dose is large one should, in principle, correct the restricted star density by removing stars due to particles entering from the tunnel. However, when one or the other dominates this will not affect the final answer greatly. Again, if need be, one can exclude restricted stars due to tunnel entrants. For relatively thin shields one should also evaluate the regular ‘CASIM dose’ at the exit point, i.e., the dose in the absence of the penetration. In the narrow-penetration- approximation this simply adds to the other components.

2.6 Low Energy Dose

Energetic particles which interact inelastically with a nucleus typically leave behind enough energy for the remaining nucleus to de-excite by emitting 'evaporation' particles. The energy of evaporation neutrons is typically a few MeV. Charged particles have higher energy but will nonetheless stop very quickly and can therefore be neglected in the present context. In ordinary CASIM evaporation neutrons are not followed explicitly but are included—on average—in the star density to dose conversion. This shortcut is justified in regions where a cascade equilibrium exists. These neutrons are included here explicitly because: (1) a penetration, especially one connected to the accelerator enclosure, tends to sample more of the earlier generations of the shower—away from the equilibrium condition, and (2) the isotropic emission of the neutrons differs strongly from the production of CASIM particles.

The low energy neutron algorithm again uses the geometry of an evacuated cylinder in a slab and relies on the (unrestricted) star densities calculated in the first stage. This contribution is evaluated as the integral:

$$\int_0^W \int_{r_p}^{\infty} \frac{\rho_*(T) n \exp(-\ell/\Lambda) 2\pi r dr dT}{L^2} \quad (8)$$

where ρ_* is the unrestricted star density, n is the average number of evaporation neutrons emitted from a struck nucleus (for concrete or soil $n = 0.8$ is assumed based on systematics [7] and on Monte Carlo results [8]), $\ell = L(r - r_p)/r$ is the distance traversed through material by the neutron with $L = \sqrt{(W - T)^2 + r^2}$ being the total length to the exit of the penetration, and $\Lambda = \tau_{1/2}/\ln 2$ where $\tau_{1/2}$ is the 'half-value thickness' for neutrons in the material (taken as 5cm for concrete [9]). In all cases studied so far this component has been negligible compared to the rest of the dose.

3 Comparisons with Measurement

Comparisons of CASIM-plus-algorithm with three measurements of deliberately induced 8GeV proton beam loss are presented. Two are of a duct-type geometry and the third is for a culvert. These measurements belong to a series intended to provide some empirical grounds for worst case beam losses around the Fermilab accelerator complex. While perhaps better reproducible than a typical radiation 'field measurement', they should not be considered as rigorously controlled experiments.

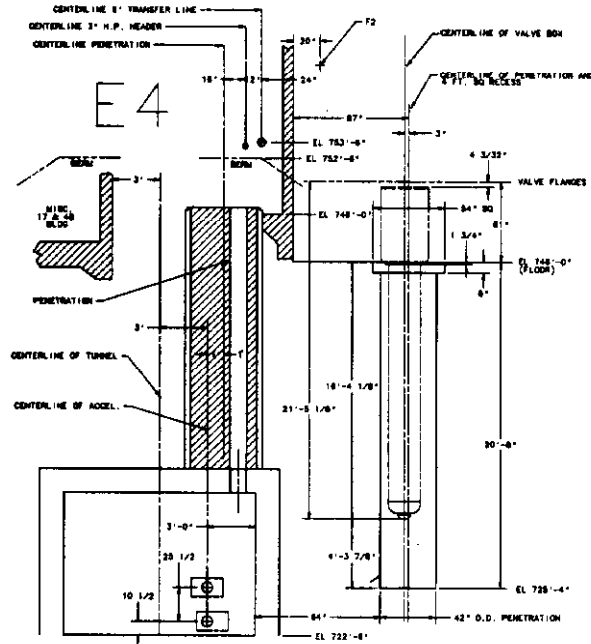


Figure 5: Elevation view of ER penetration.

3.1 ER Penetration

This compares calculated and observed exit dose for a duct which runs from the ER enclosure to the Fermilab Main Accelerator tunnel in the vicinity of station E4. Fig. 5 shows a design (elevation) drawing in the plane of the penetration. Beam losses are induced—and the dose at ER is then maximized—by varying magnet strengths in that vicinity. The long straight section which runs by the penetration is only sparsely equipped with magnets and other apparatus. Such an arrangement is expected to be quite sensitive to detail of beam loss and may be capable of producing close to a worst case dose, expected when cascade development and self-shielding are in optimal balance. Since a reliable description of the beam loss is lacking, and in view of the empirical dose maximization, it appears reasonable to replace the complicated geometry of the straight section with an equivalent ‘worst case iron cylinder’. [10]

The shield dose is calculated for a cylindrically symmetric $r = 7\text{cm}$ iron target in a $r = 190\text{cm}$ tunnel with a wall of standard (Fermilab) soil ($\rho = 2.24\text{g/cm}^3$). The duct is in a plane perpendicular to the beam and

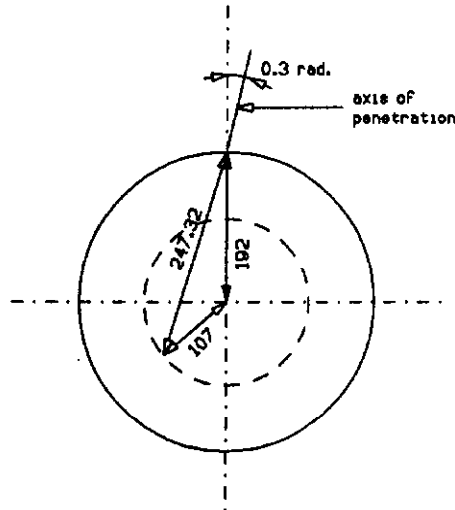


Figure 6: Simplified geometry to calculate tunnel dose of ER penetration. Distances are in *cm*.

is oriented at an angle of 0.3 radians with respect to the radius vector at its entrance to the tunnel. The solid angle limits imposed on the restricted star density are: $-0.1 < d_z < 0.1$ where d_z is the direction cosine of the particle creating the star with respect to the beam and $-0.1 < \phi - \phi_0 < 0.1$ where ϕ is the angle between particle direction and radius vector and ϕ_0 is the angle between penetration and radius vector at the point where the star is created. For convenience the tunnel dose is calculated separately with a somewhat different geometry. The cascade trajectories contributing to this dose must enter the wall opposite the penetration, re-emerge, cross the tunnel and strike the wall at the correct angle with respect to beam and radius vector. The full 2π azimuthal range can be exploited by the artifice of making the geometry dependent upon the history of a cascade trajectory. Thus the first time a tunnel wall is encountered by such a trajectory is at $r_1 = 107\text{cm}$; if it re-emerges then for any subsequent encounter(s) the tunnel wall is placed at $r_2 = 192\text{cm}$. From fig. 5 $r_1 = 107\text{cm}$ represents the distance from the beam to a spot on the floor directly underneath the duct. Since the floor-to-ceiling distance is 274.3cm (9ft) it follows (fig. 6) that r_2 must be 192cm . The solid angle limits are the same as above. Finally the plain CASIM dose, without penetration, obtained from the unrestricted star density, is added to the above components. For wide penetrations this will tend to overestimate the dose, but here (for $r = 15\text{cm}$) this bias is probably not significant.

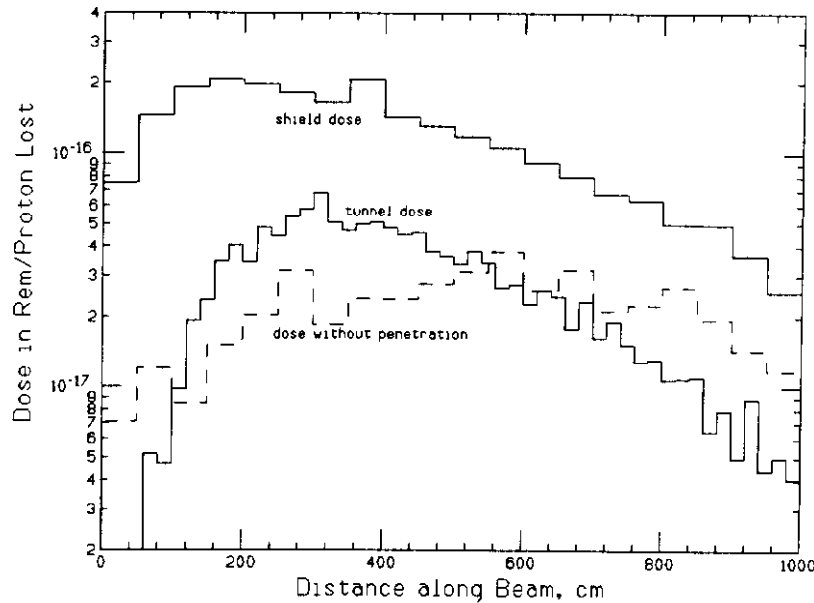


Figure 7: Exit dose at ER as a function of distance from point of beam loss.

Fig. 7 shows the results of the calculation with the different components of the exit dose plotted as a function of z . As can be seen the maximum dose equivalent predicted is about $2.5 \cdot 10^{-16}$, as compared with a measured value of $1.55 \cdot 10^{-16} \text{ rem}$ per proton lost. The overestimate is likely the result of representing the straight section by an $r = 7 \text{ cm}$ iron cylinder. As noted above this is done for expediency, and no attempt has been made to evaluate the closeness of this approximation. In any case, one expects a worst case target to overestimate the dose and a factor of 1.6 is not unreasonable.

3.2 Booster Transfer Line

This comparison deals also with ducts but differs considerably from the previous case. In contrast with the ER penetration the beam loss is relatively well defined. There are *two* ducts which are both much longer and more radially oriented compared with the ER case. Fig. 8 shows a plan view of the accelerator layout in this vicinity. Beam is bent up by 50 mrad starting at magnet VB1 and as a result strikes magnet QDC5 some 5 cm below the top. A 4 in. diameter beampipe— 0.080 in. thick—is present. Radiation dose is measured at the top of the shielding penetrations which are elevated about

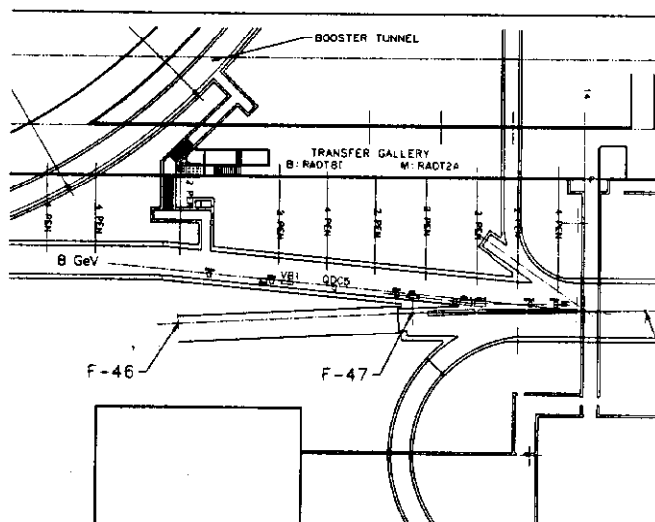


Figure 8: Plan view of accelerator layout in vicinity of station F47.

15ft above the beam. Only the ducts marked B:RADT8A and M:RADT2A at the exit are of interest here.

The calculation proceeds much like for the above case. The bending magnet does not intercept the beam and can be omitted. The beam strikes the beampipe *en route* to QDC5 where its height is lowered by 29cm. This allows QDC5 to be reduced to a cylindrical iron target of $r = 11cm$, which represents an estimated distance through the magnet along the beam-duct direction. Elsewhere the bare beampipe is present. As seen from fig. 8 the ducts are not quite perpendicular to the beam and a direction cosine of -0.1 with respect to the beam is assumed. The angle of the duct with the radius vector in the (x, y) -plane is assumed to be 0.1 radian at the tunnel radius. The ducts vary in length and in cross-sectional area with $l = 1280cm$ and $\sigma = 565cm^2$ for '2A' and $l = 1220cm$, $\sigma = 1130cm^2$ for '8I'. It should be noted that the duct cross sections are rectangular in shape: roughly $7in. \times 12.5in.$ and $7in. \times 25in.$ for 2A and 8I, respectively. They are partitioned, by $0.5in.$ concrete dividing walls which run parallel to the $7in.$ side, into two and four compartments, respectively. For the shield dose the tunnel is assumed to have a $340cm$ radius which corresponds to the (average) distance from beam to penetration. The shield is again assumed to be of standard Fermilab soil. For the tunnel dose the same type of trajectory-dependent geometry is assumed as for ER with the two walls

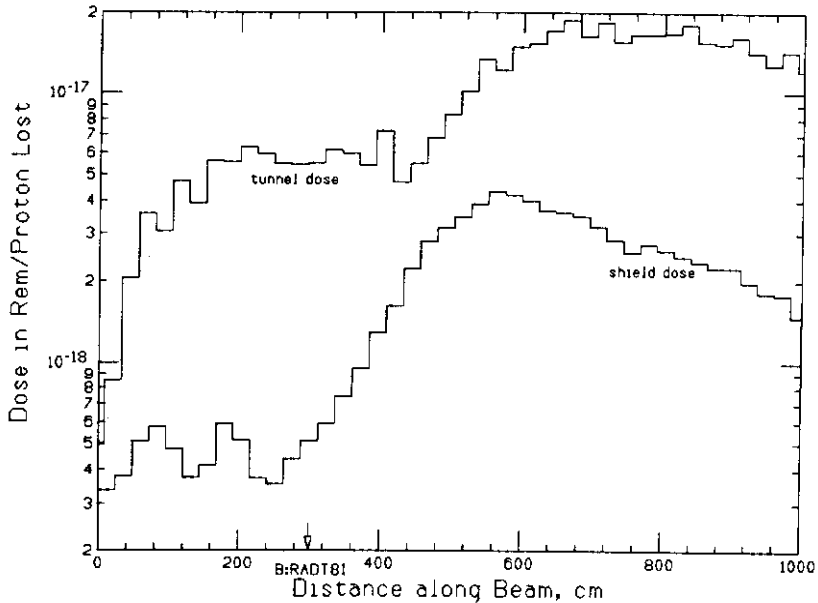


Figure 9: Exit dose for penetration with cross section area of 1130cm^2 as a function of distance along the beam (measured at exit). Actual penetration is marked at about 300cm .

placed at 60cm and 340cm respectively. The ± 0.1 limit on d_z is retained but—because the duct is nearly radial—the angle between particle direction and radius vector is required to be within ± 0.05 radians. The CASIM dose without penetration is negligible here.

Results are shown again as a dose versus distance plot in fig. 9 for the 8I duct. Distance is measured along the outside of the shield from the point corresponding to where beam is bent upward, which puts the center of 8I at $z = 300\text{cm}$. The total estimated dose at this point is $5.5 \cdot 10^{-18}$ as compared with an observed $1.67 \cdot 10^{-18}\text{rem}$ per proton lost. Fig. 10 is a comparable plot for the 2A duct, which is at 900cm from the bend center. The total dose calculated at this point is $7.8 \cdot 10^{-18}$ vis-a-vis an observed $5.1 \cdot 10^{-18}\text{rem}$ per proton lost. The calculation comes much closer at 900cm than at 300cm . Possible reasons for this discrepancy may be the representation of the $7\text{in.} \times 25\text{in.}$ penetration as circular and ignoring the presence of the dividing walls. This could also affect the 900cm result but to a lesser extent. This is in line with the magnitudes of the respective discrepancies. Aside from this one could also improve on modeling the geometry.

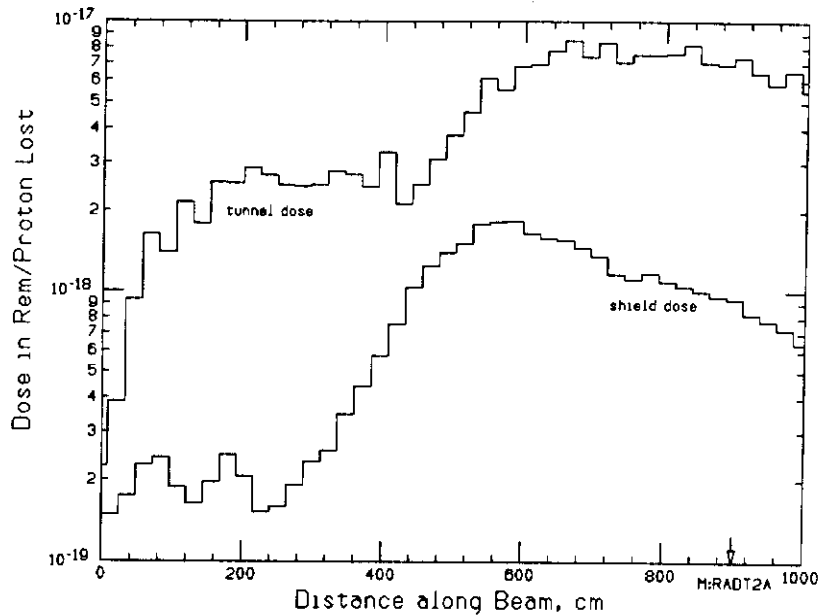


Figure 10: Exit dose for penetration with cross section area of 565cm^2 as a function of distance along the beam (measured at exit). Actual penetration is marked at about 900cm .

3.3 C39 Culvert

The final comparison presented here is between calculated and observed dose outside a culvert which crosses the berm in the proximity of station C39. Fig. 11 shows a cross section of the geometry. The culvert has a large, rectangular cross section which measures $2\text{ft} \times 12.67\text{ft}$ overall and is divided in half by a vertical 1ft thick wall. These dimensions certainly exceed the bounds of the narrow penetration assumption. The geometry is readily symmetrized with only the off-center position of the beam in the 'horseshoe' to be rectified. The shortest distance from beam to culvert is about 374cm of which 154cm is inside the tunnel (close to the 151.5cm actual horseshoe radius). This suggests taking a circular tunnel of 154cm with beam running along the center and with the culvert 374cm away at closest approach. The distance along the culvert from this last point to where dose is measured is about 900cm . The culvert is represented by a circular tunnel with area equal to (both sections of) the culvert. As in the ER case, beam loss is maximized with respect to the dose measurement. Since the

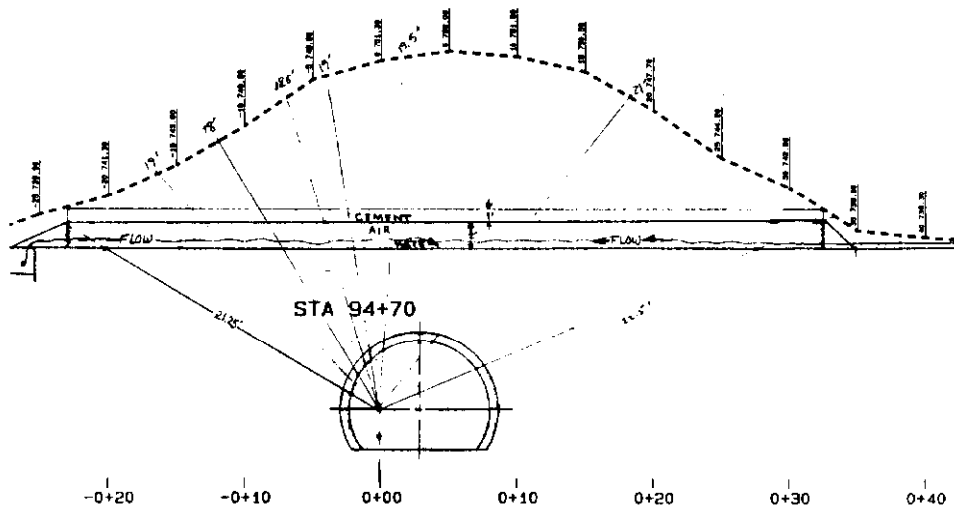


Figure 11: Geometry of culvert at C39.

accelerator components nearby are those of the standard arc lattice, beam loss is simulated by letting the beam strike a Main Ring dipole at an angle of 2.4mrad as estimated from the magnet settings. There is no tunnel dose and the dose without penetration is negligible.

Fig. 12 shows the dose as a function of distance along the beam direction. At its maximum this can be seen to equal about $3.0 \cdot 10^{-18}$ as compared with an observed $3.8 \cdot 10^{-18}$ rem per proton lost. The agreement to within 20% is quite gratifying.

4 Concluding Remarks

As shown in the preceding section results of the algorithm compare reasonably well with measurements. Given the additional uncertainties associated with modeling a duct or culvert, agreement is in line with that of plain CASIM for shields of comparable radial extent. Some of the (over-) symmetrizing in modeling the geometry and beam loss corresponding to the measurements may tend to devalue the comparisons somewhat. This is less of a problem for estimating worst case dose rates which preferably should not be strongly dependent on geometry or phase space distribution of the lost beam. One therefore reverts, almost of necessity, to a 'worst case' cylindrical target. [10]

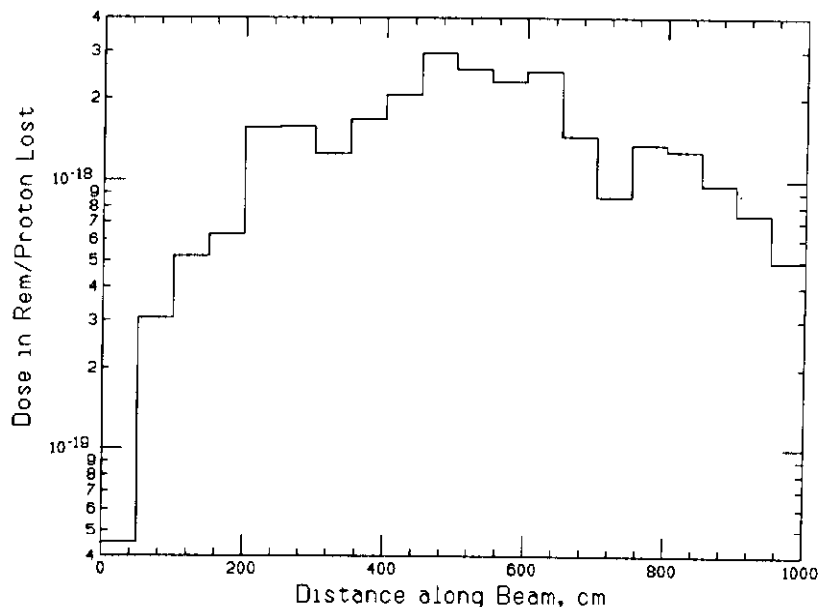


Figure 12: Exit dose at C39 culvert as a function of distance along the beam from point of beam loss.

So far the present algorithm has been applied only to single straight labyrinths. One can easily envision its extension to straight multi-legged ones. In addition to the exit dose, the analysis then should include possible 'soft spots' in the shielding, i.e., points where the axis of a (buried) labyrinth leg crosses the shielding berm. For sufficiently long multi-legged labyrinths where one is sure on *a priori* grounds that only the low energy neutron *exit* dose is significant, the present treatment can be combined with the usual labyrinth rules [3]. The above algorithm may be used to calculate the dose at the 'corners' of the penetration up to a point where dose entering through the walls is negligible, and the labyrinth rules can then be invoked to attenuate the dose from each corner through the rest of the labyrinth.

Statistics could be improved significantly by calculating for each star the number of particles traveling in the 'right' direction with respect to z and τ —instead of merely noting whether it does or not. This has the further advantage that the step of calculating the particles contributing to the dose could be uncoupled from the cascades program. One could try different production models, especially those most reliable at lower energy. Even a minimal implementation of this would require much more extra effort com-

pared with the present CASIM 'patch'. However, given the encouragement derived from comparisons of the latter with measurements these improvements are worth considering. With this approach one may also afford to relax—at least in part—the sometimes awkward imposition of cylindrical symmetry on the problem.

My thanks to C. Crawford, D. Finley, K. Koepke, S. Pruss, and their coworkers for making the results of the measurements available and for helping me interpret the associated geometries. Thanks also to C. Ankenbrandt for his comments on the manuscript.

References

- [1] A. Van Ginneken, CASIM. Program to Simulate Hadronic Cascades in Bulk Matter, Fermilab FN-272 (1975).
- [2] Throughout, for brevity, 'dose' refers to dose equivalent.
- [3] For a recent review of such calculations see, e.g, G. R. Stevenson, CERN preprint TIS-RP/182/CF (1987).
- [4] The flux-to-dose conversion constant c_ϕ is related to c_* the star-to-dose conversion factor: $c_\phi = c_*/\lambda$, where λ is the absorption length in the medium. For concrete c_* is usually taken as $9 \cdot 10^{-6} \text{rem/star} \cdot \text{cm}^3$ in CASIM calculations. For soil the corresponding constant is $1.03 \cdot 10^{-5}$. These constants include dose due to low energy particles ($< 50 \text{MeV}$) which are assumed to accompany the CASIM particles and to be in equilibrium with them. For more detail on these particular conversion factors see A. Van Ginneken and M. Awschalom, High Energy Particle Interactions in Large Targets, Fermilab, Batavia, IL (1974). These factors are not universally agreed upon, see, e.g., K. Tesch and H. Dinter, Radiation Protection Dosimetry, 15, 89 (1986) and G. R. Stevenson, CERN preprint TIS-RP/183/CF (1987). In sec. 3 the usual CASIM conversion constants are used.
- [5] W. Feller, An Introduction to Probability Theory and its Applications, Vol. II, Wiley, New York (1966).
- [6] Care must be taken when T approaches W . Eq. (1) should be modified to include radial distance but in most cases one can neglect this region altogether since star density drops exponentially with T .

- [7] see, e.g., M. A. Preston, *Physics of the Nucleus*, Addison -Wesley, Reading, MA (1962).
- [8] H. W. Bertini, *Phys. Rev.* **188**, 1711 (1969).
- [9] R. Wallace, *Nucl. Inst. Meth.*, **18/19**, 405 (1962).
- [10] In the context of penetrations it is reasonable to use a long cylindrical iron target with a radius, r , of about 7cm . It has been found empirically, from a series of CASIM runs, that when the target radius is varied, the maximum star density (ρ_*^{max}) at the inside tunnel wall (of 1m radius) as a function of r , exhibits a broad maximum at $r = 7\text{cm}$ with little variation between $r = 2\text{cm}$ and $r = 12\text{cm}$. The maximum broadens further when one plots ρ_*^{max} at larger radii—inside the tunnel wall.